Published by :
http://www.ijert.org

International Journal of Engineering Research & Technology (IJERT)
ISSN: 2278-0181
Vol. 13 Issue 06, June - 2024

# Development of the Minimum Ray Distance Algorithm for the Orientation of Spherical Panoramic Images

Naa Dedei Tagoe
Department of Geomatic Engineering, University of Mines and Technology, Tarkwa, Ghana

Yakubu Issaka
Department of Geomatic Engineering, University of Mines and Technology, Tarkwa, Ghana

***Abstract*—Rapid advancements in imaging technology and relatively affordable, conventional digital cameras have contributed to the growing interest in panoramic imaging and photogrammetry. However, accurately orienting and reconstructing 3D objects from panoramic images poses significant challenges. This paper presents the development of an accurate close-range photogrammetric technique for the semi-automatic extraction of 3D information from spherical panoramic images. This was achieved by developing an algorithm referred to as the Minimum Ray Distance (MRD) for the fully automated approximate relative orientation of spherical panoramic images. Prior to orientation, the image coordinates of conjugate points on the panoramic images are measured either manually or automatically using a feature-based matching technique. The bundle adjustment algorithm was then applied to refine the orientation parameters of the panoramic images, enabling accurate 3D point measurement. The epipolar geometry was applied to the oriented panoramic images to guide the interactive extraction of additional conjugate points. The bundle adjustment was then used again to refine the 3D coordinates of additional points. The validity and accuracy of the approach were tested using the Calibration Testfield at the University of Cape Town's Photogrammetry Laboratory and on several cultural heritage sites including Fort Jago, a UNESCO World Heritage Site in Ghana.**

***Keywords*— spherical panoramic images, panorama; the Minimum Ray Distance algorithm, orientation, epipolar geometry**

## I. INTRODUCTION

Spherical panoramic images have become increasingly prevalent in various fields, including cultural heritage preservation and urban planning, due to their ability to capture detailed spatial information. However, accurately orienting and reconstructing 3D objects from panoramic images poses significant challenges. Early researchers mostly relied on cylindrical panoramic images generated from rotating line panoramic cameras [1, 2] or spherical panoramic images generated by stitching images captured with conventional cameras and rectilinear lenses [3, 4].

The photogrammetric processing of panoramic images, generally referred to as Spherical Photogrammetry, was introduced by G. Fangi [3]. In Spherical Photogrammetry, the bundle adjustment algorithm is used to simultaneously determine the exterior orientation parameters (EOPs) of the panoramic images and the 3D coordinates of the object points [1-4]. The mathematical model of the bundle adjustment algorithm, however, is non-linear, thus requiring good initial approximations. Maas and Schneider [2] obtained initial approximations by applying sequential Cassini-resection and spatial intersection. This approach to generating initial approximations for the exterior orientation parameters relies on the known coordinates of control points. This makes the orientation phase cumbersome and time-consuming, especially for non-technical operators. Fangi [3, 4] generated initial approximations by applying relative orientation based on the coplanarity equations, followed by the transformation of independent models into a global coordinate system. Like the collinearity equations, the coplanarity equations are non-linear. Therefore, they require good initial approximation values to solve the unknown parameters. Fangi [3, 4] resolved this challenge by defining arbitrary values for unknowns (orientation angles). The approximation values are subsequently refined until the iterative least squares computation converges. This process of defining the approximation values for the unknown parameters makes the orientation procedure for spherical panoramic images cumbersome. Henceforth, the term 'spherical panorama' will be used interchangeably with 'spherical panoramic images'.

This paper addresses these challenges through the development of the Minimum Ray Distance (MRD) algorithm for initial orientation, followed by bundle adjustment techniques for refinement of object coordinates. The methodology includes feature extraction, matching based on epipolar geometry, and scaling corrections to enhance the accuracy of 3D reconstructions from panoramas. Special emphasis was placed on developing an orientation procedure for generating initial approximation values for exterior orientation parameters. The initial approximation values required to solve the exterior orientation parameters in the research are neither arbitrarily defined nor does the orientation procedure rely on the coordinates of known control points.

Published by :
http://www.ijert.org

International Journal of Engineering Research & Technology (IJERT)
ISSN: 2278-0181
Vol. 13 Issue 06, June - 2024

## II. MATERIALS AND METHODS

### A. Study Area

The approach to extracting 3D information from spherical panoramas via the MRD algorithm was tested on the Calibration Testfield at the University of Cape Towns' Photogrammetry Laboratory. The laboratory covers a floor area of 8 m by 8 m and is about 3 m in height. The Calibration Testfield consists of a near-planar point array of 91 targeted calibration points with known 3D object coordinates. The target points of the Calibration Testfield are well distributed over a wall area of approximately 6 m by 2.5 m on one side of the room. These points are represented by circular targets in the form of white retro-reflective disks of 14 mm diameter on a black background (Figure 1), whose 3D object coordinates were determined using a theodolite.


Fig. 1 Calibration Testfield at University of Cape Town

### B. Materials Used

The materials used in this study include a Nikon D200 DSLR camera with a Nikkor 10.5 mm fisheye lens for capturing spherical panoramas. The coding of the feature extraction and image matching processes, the MRD and bundle adjustment algorithms and 3D Helmert Transformation were programmed in MATLAB. A total station was used to accurately measure the 3D object coordinates of these targets, which were determined with sub-millimetre accuracy from a three-point base triangle.

### C. Development of the Minimum Ray Distance Algorithm

The underlying concept of the MRD algorithm is the minimisation of distances between two conjugate space vectors or skewed rays. This approach is based on the premise that the vectors from the centre of separate panoramas ($\boldsymbol{PC1}$ and $\boldsymbol{PC2}$) to the same object point (P) intersect at this point, albeit not perfectly because of observation and other errors. The panoramas' unknown orientation and relative positions and heights can be determined iteratively by stepwise rotating the un-oriented panoramas with respect to each other and by iteratively changing the height displacements between the panoramas until a global minimum distance between conjugate rays is achieved. Rotations are iterated around the three coordinate axes by angles omega ($\boldsymbol{\omega_i}$), phi ($\boldsymbol{\phi_i}$) and kappa ($\boldsymbol{\kappa_i}$). If $\mathbf{L1}$ and $\mathbf{L2}$ are conjugate rays defined by the vectors $\vec{\boldsymbol{u}}$ and $\vec{\boldsymbol{v}}$ respectively, then the minimum distance between the two rays after each rotation is found between points $\boldsymbol{Pa_{(s)}}$ and $\boldsymbol{Pb_{(t)}}$ where the two vectors $\vec{\boldsymbol{u}}$ and $\vec{\boldsymbol{v}}$ have a common normal (Figure 2). The minimum distance between the rays $(\mathbf{L1}, \mathbf{L2})$ is mathematically expressed as follows:

$$\boldsymbol{d(L_1, L_2)} = \min_{\boldsymbol{Pa_{(s)}} \in \boldsymbol{L_1}\, \boldsymbol{Pb_{(t)}} \in \boldsymbol{L_2}} \{\boldsymbol{d(Pa_{(s)}, Pb_{(t)})}\} \qquad (1)$$

such that, $\boldsymbol{L1 = PC1 + s\vec{u}}$, and $\boldsymbol{L2 = PC2 + t\vec{v}}$. The mid-point between the two points, $\boldsymbol{Pa_{(s)}}$ and $\boldsymbol{Pb_{(t)}}$ defines the 3D position of the object point $\boldsymbol{(X_j, Y_j, Z_j)}$.

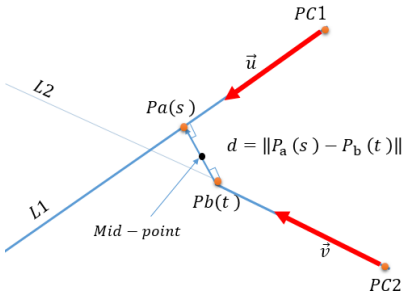


Fig. 2 Minimum distance between two skew rays

Figure 3 shows a typical setup of two panoramas before and after relative orientation by MRD algorithm.

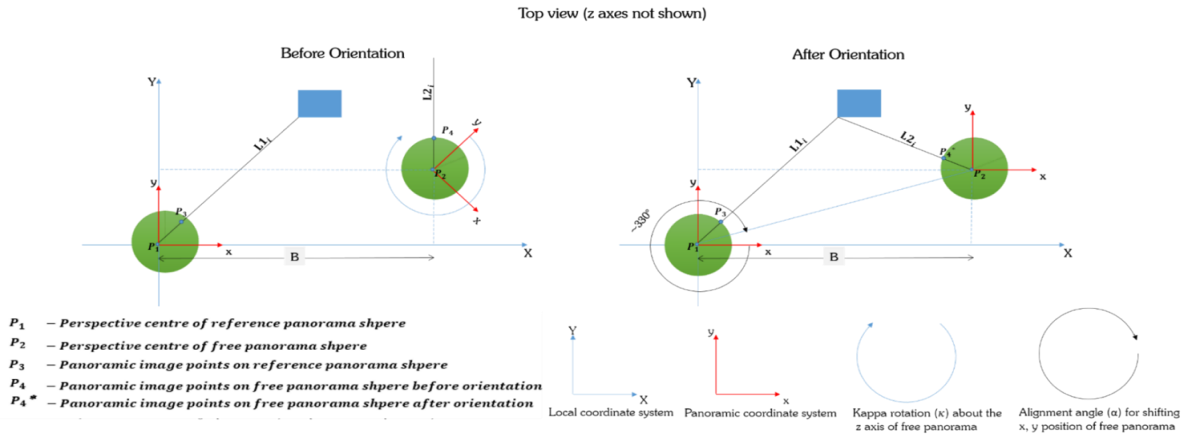


Fig. 3 MRD algorithm configuration

International Journal of Engineering Research & Technology (IJERT)
ISSN: 2278-0181
Vol. 13 Issue 06, June - 2024

The minimum distance is evaluated for one ray and a bundle of rays from each panorama centre.

- **PC1** and **PC2** are the perspective centres of the reference and free panoramas, respectively.
- $\mathbf{PC1}_i$ and $\mathbf{PC2}_i$ represent the 3D coordinates of object points on the reference and free panorama spheres; the coordinates of $\mathbf{PC2}_i$ are modified in the iteration process.
- Provisional base ($\boldsymbol{B}$) is the arbitrarily chosen distance between the reference and free panoramas. The actual scale of the derived model will be determined later by measuring or calculating an object distance from known coordinates.

Prior to the implementation of the MRD algorithm, no information about the relative position and height of the panoramas is known. EOPs $(X_{o1}, Y_{o1}, Z_{o1}, \omega_1, \phi_1, \kappa_1)$ and $(X_{o2}, Y_{o2}, Z_{o2}, \omega_2, \phi_2, \kappa_2)$, are therefore assumed as (0,0,0,0,0,0) and (0,B,0,0,0,0) for the reference and free panoramas respectively. It is also assumed that the panoramas are "quasi-horizontal" *i.e.* within 10º horizontal.

The task of the MRD algorithm is to estimate the EOPs for the free panorama(s) and object coordinate values for all image points (Figures 4 and 5).

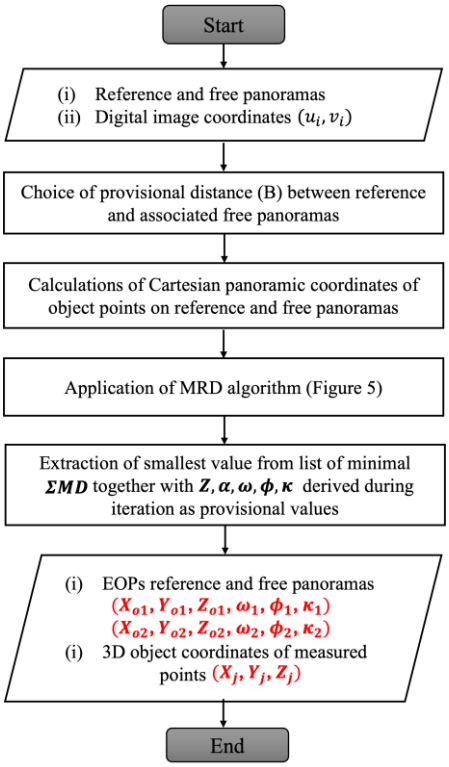


Fig. 4 Overview of automatic estimation algorithm for the creation of initial approximation values for bundle adjustment

This involves keeping the EOPs of the reference panorama fixed while the 2D position $(\boldsymbol{X}, \boldsymbol{Y})$, height $(\mathbf{Z})$ and the three rotational angles $(\boldsymbol{\omega}, \boldsymbol{\phi}, \boldsymbol{\kappa})$ of the free panorama are varied in steps. To initiate the iterative orientation process, the default value for the provisional base is chosen as 1 or as a rough realistic estimation of the actual base, the height range for the iteration is then set equal to the base, B allowing iteration for the height to step through values from –B to +B in steps of B/10.

Figure 6 shows the hill-climbing approach [5] for the determination of the height $(\mathbf{Z})$ of the panoramas.

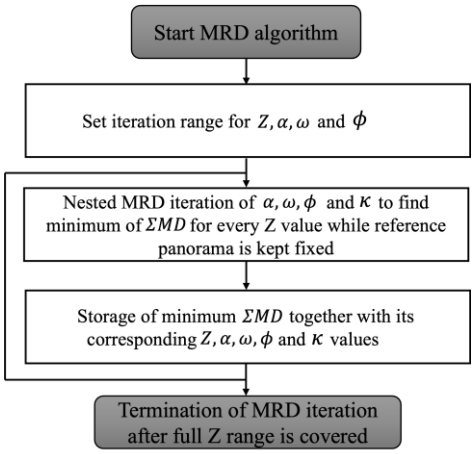


Fig. 5 MRD algorithm

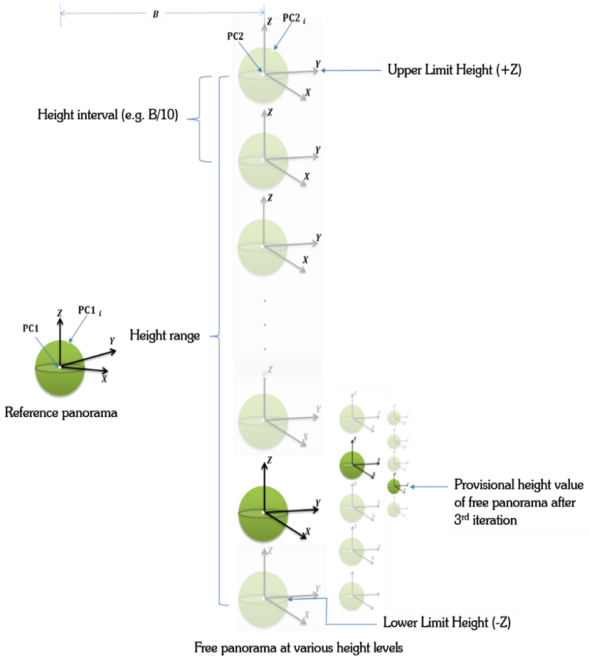


Fig. 6 Height determination for the free panorama using the MRD algorithm

The 2D position of the free panorama $(\boldsymbol{X_2}, \boldsymbol{Y_2})$ is obtained by varying the 'alignment angle' $(\alpha)$ (Figure 7).

It should be noted that there are two rotational angles, $\boldsymbol{\alpha}$ is the rotation of the base from its starting position, and κ is the rotation of the free panorama about its centre . The iteration for rotational angle $\boldsymbol{\kappa}$ ranges from 0° to 360° in intervals of 1° or 5°, and the iteration for rotational angles $\boldsymbol{\omega}$ and $\boldsymbol{\phi}$ ranges from -10° to +10° in intervals of 1°. The three angles and the height difference can be refined using smaller steps within a limited range (narrower search space) around the previous approximation.

International Journal of Engineering Research & Technology (IJERT)
ISSN: 2278-0181
Vol. 13 Issue 06, June - 2024

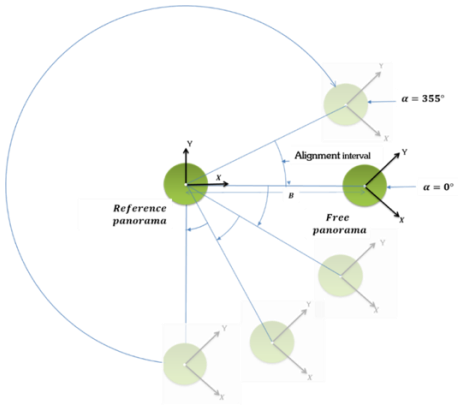


Fig. 7 Determining suitable alignment angle for the 2D position of free panorama.

As mentioned above, for each iteration step, the minimum distance $s(\boldsymbol{d})$ between the conjugate rays ($\mathbf{L1}_i$ and $\mathbf{L2}_i$) are determined for all image points (Figure 2 and Equation 1). The $\boldsymbol{Z}$, $\boldsymbol{\omega}$, $\boldsymbol{\phi}$ and $\boldsymbol{\kappa}$ values associated with the global minimum of the sum of all minimum distances indicate the optimal position and orientation between the two panoramas. The mid-point between the point vectors $\boldsymbol{Pa}_{(s)}$ and $\boldsymbol{Pb}_{(t)}$ then define the provisional values for 3D coordinates of the object points $(\boldsymbol{X_j}, \boldsymbol{Y_j}, \boldsymbol{Z_j})$.

D. Epipolar Geometry of Spherical Panoramas

A spherical panorama captures a complete 360° horizontal view and a 180° vertical view of a scene. On the panorama sphere (Figure 8 and 9), two coordinate systems can be defined. These are the Cartesian panoramic $(\boldsymbol{x_i}, \boldsymbol{y_i}, \boldsymbol{z_i})$ and spherical $(\boldsymbol{\lambda_i}, \boldsymbol{\phi_i})$ coordinate systems. The relationships between the two systems are as follows (Equations 2-6):

$$x_i = r \ \sin\lambda_i \sin\phi_i \qquad (2)$$

$$y_i = r \ \cos\lambda_i \sin\phi_i \qquad (3)$$

$$z_i = r \ \cos\phi_i \qquad (4)$$

The inverse solutions are expressed as:

$$\lambda_i = \arctan\left(\frac{x_i}{y_i}\right) \qquad (5)$$

$$\phi_i = \arccos\left(\frac{z_i}{r}\right) \qquad (6)$$

where $\boldsymbol{\lambda_i}$ represent the latitude, $\boldsymbol{\phi_i}$ is the longitude and $\boldsymbol{r}$ is the radius of the sphere. To map spherical panoramas onto a flat image plane (Equation 7 and 8), the Equirectangular projection is commonly employed [3,6].

$$u_i = r\,\lambda_i \qquad (7)$$

$$v_i = r\,\phi_i \qquad (8)$$

This projection facilitates the visualisation and analysis of the spherical panorama in a conventional 2D format. Fangi and Nardinocchi [7] investigated the epipolar geometry for spherical panoramas using synthetic images. To automate the 3D coordinate extraction process after panorama orientation, the epipolar geometry of the spherical panorama was implemented in this research on real images. The epipolar geometry of the panorama pair reduces the search space from a full 2D image space image to 1D (epipolar curve). Figure 8 shows the epipolar geometry between two oriented panorama spheres where P an object point in space is.

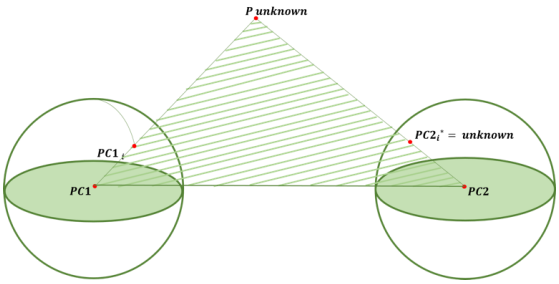


Fig. 8 Epipolar geometry between two oriented spherical panoramas

The intersection of the epipolar plane, defined by PC1, PC2 and P, through the two oriented panorama spheres, creates great circles on each of the panorama spheres (Figure 9). These great circles appear as sinusoidal curves on the spherical panoramas and are known as epipolar curves (Figure 10).

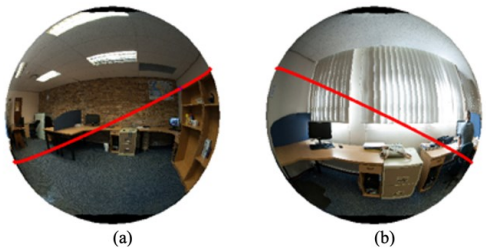


Fig. 9 Intersection of epipolar plane with a panorama sphere defining a great circle (a) Front view (b) Back view

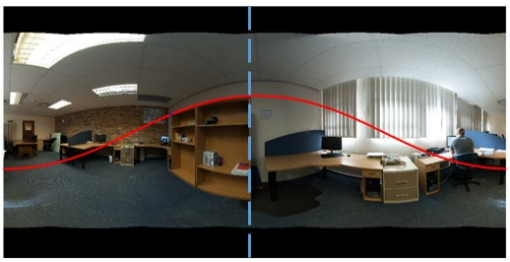

Fig. 10 Epipolar curve on the panoramic image plane

To derive the mathematical formula for the epipolar curve on the panoramic image plane, the general equation of the plane is used (Equation 9).

International Journal of Engineering Research & Technology (IJERT)
ISSN: 2278-0181
Vol. 13 Issue 06, June - 2024

$$Ax + By + Cz = \mathrm{n} \cdot \mathrm{x} = 0 \quad (9)$$

where $\begin{bmatrix} A \\ B \\ C \end{bmatrix}_{1,3}$ is normal vector to the plane and $\begin{bmatrix} x \\ y \\ z \end{bmatrix}_{1,3}$ represent the Cartesian panoramic coordinates of any point on the sphere. By substituting Equation 2 to 4 into Equation 9, the epipolar plane expressed in spherical coordinates is given as:

$$A * r \sin\lambda \sin\phi + B * r \cos\lambda \sin\phi + C * r \cos\phi = 0 \quad (10)$$

From Equation 10, the expression for the great circle, expressed in spherical coordinates as [7]:

$$\phi = arctan\left(\frac{-C}{A*\sin\lambda + B*\cos\lambda}\right) \quad (11)$$

where $\boldsymbol{A}, \boldsymbol{B}$ and $\boldsymbol{C}$ are the elements of the normal vector and $\boldsymbol{\lambda}$ is the horizontal angle of the points, which ranges from 0° to 360°.

Finally, the expression for the epipolar curve on the panoramic image plane is obtained by substituting the equation for $\boldsymbol{\lambda}$ (5) into Equation 11.

$$v = r * arctan\left(\frac{-C}{A*\sin\left(\frac{u}{r}\right) + B*\cos\left(\frac{u}{r}\right)}\right) \quad (12)$$

While the epipolar geometry of a panorama pair reduces the search space from the complete 2D image space to a 1D epipolar curve, the search space can be further reduced to a single point if two or more oriented panoramas are available, in which case the search is fully automated**.** Figure 11 shows an example of the extraction of a feature point on a 2D panoramic image with the support of the epipolar geometry after the relative orientation of four panoramas.

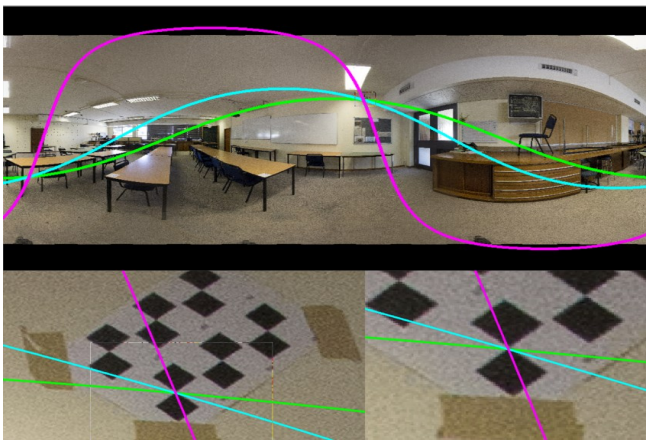

Fig. 11 Interactive extraction of a feature point from a 2D panoramic image supported by epipolar geometry after relative orientation of four panoramas shown at different zoom levels

Three epipolar curves are plotted on the single panorama intersect at two points, one in the upper-half of the panorama and the second in the lower-half. The point in the lower half is automatically eliminated based on the minimum distance between two conjugate rays (Equation 1).

E.Orientation of Spherical Panoramas by the MRD Algorithm
Prior to orientation, image coordinates of conjugate points on the panoramas are measured either manually or automatically. Automatic conjugate point extraction is accomplished by a feature-based matching technique based on the Scale Invariant Feature Transform (SIFT) operator [8, 9] whiles the Random Sample Consensus (RANSAC) algorithm was used to remove outliers from the dataset [10]. To avoid excessive computation time, a subset of the extracted conjugate points is used as input in the MRD algorithm. Typically, some six to ten conjugate points suffice to provide the initial approximation values required for the bundle adjustment. The workflow for the panorama orientation and extraction of 3D coordinates of object points involves five principal routines (Figures 12 and 13). These are the MRD and bundle adjustment algorithms, scaling of object coordinates, interactive extraction of conjugate points guided by the epipolar geometry and 3D similarity transformation. First, the MRD algorithm is sequentially applied to pairs of spherical panoramas to automatically estimate the initial approximation values for the unknown parameters. This is followed by scaling all derived object coordinates to a common uniform scale. The bundle adjustment algorithm is then carried out to jointly refine the initial approximation values for the unknown parameters for all panoramas within a panorama configuration. A panoramic configuration in this paper refers to a group of panoramas defined within a local coordinate system, where a single panorama is selected as reference and all others, known as the free panoramas, are sequentially oriented with respect to the reference panorama. The initial approximation values for 3D object coordinates of any additional image points which were not included in the orientation phase as well as points interactively or automatically measured through the guidance of the epipolar geometry can then be calculated. The final 3D object coordinates of all image points are then determined by the bundle adjustment algorithm.
If all possible panorama connections have been formed and there are not sufficient points in the remaining panoramas, a new configuration is created. In a final step, the configurations can be linked with 3D similarity transformation which requires lesser points than the MRD orientation process. Given three or more control points with known object coordinates within a project area, the local coordinate system can then be georeferenced into the desired national or local coordinate system.

Published by :
http://www.ijert.org

International Journal of Engineering Research & Technology (IJERT)
ISSN: 2278-0181
Vol. 13 Issue 06, June - 2024

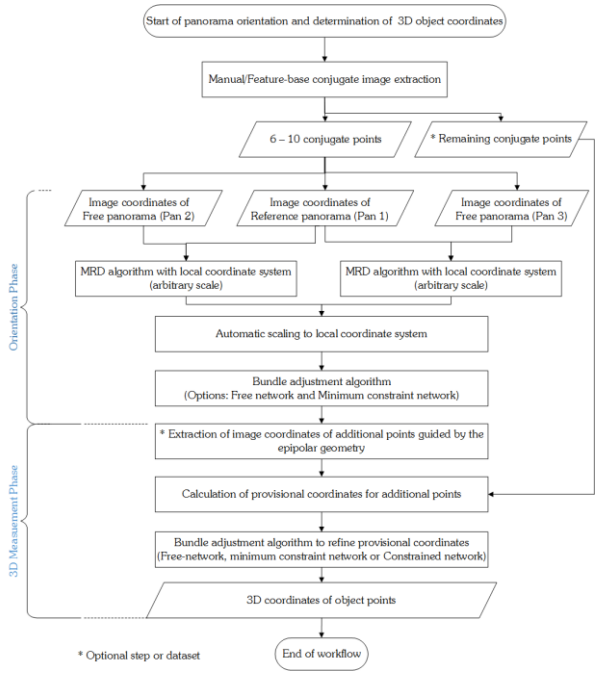


Fig. 12 Workflow for orientation and extraction of 3D coordinates of object points within a panoramic configuration

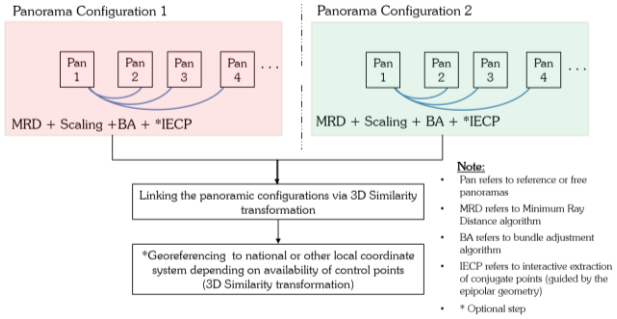


Fig. 13 Overall workflow for panorama orientation and extraction of 3D coordinates of object points

## F. Experimental Test - UCT Calibration Testfield

Four panoramas (Figure 14) were captured at random positions in the Geomatics Laboratory to determine the 3D object coordinates of the target points of the Calibration Testfield (Figure 1).

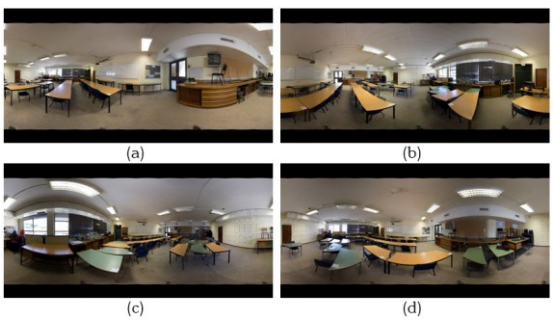


Fig. 14 Four spherical panoramas of the Calibration Testfield: (a) Panorama A (b) Panorama B (c) Panorama C (d) Panorama D

The image coordinates of fifteen points on the panoramas, eight of which were target points of the Calibration Testfield were measured manually. All fifteen points were common to the four panoramas. The approximate positions of the four panoramas relative to the image points are shown in Figure 15.

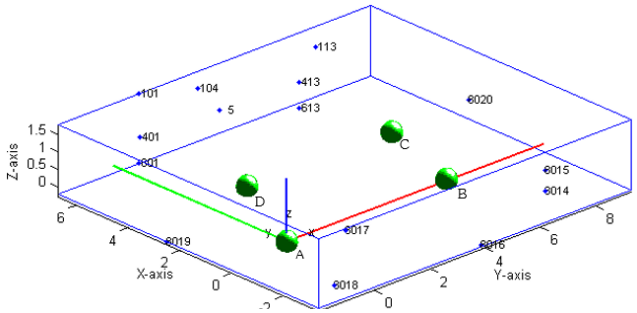


Fig. 15 Approximate positions of the four panoramas relative to the fifteen image points in the UCT Geomatics teaching laboratory

Panorama A (Figures 14a and 15) was chosen as the reference and the other panoramas were oriented and positioned with respect to it. Scaling information was derived from the distance calculated from reference coordinates of two target points 601 and 613 on the test field (Figures 1 and 15). After scaling, the initial approximation values for all EOPs are available. The bundle adjustment algorithm was applied to refine the initial approximation values for EOP of the panoramas as well as the 3D object positions of all the fifteen image points that were involved in the MRD orientation process. The epipolar geometry was used to guide the extraction of image coordinates of the remaining sixty-nine target points. The initial approximation values of targets were then calculated. Finally, the EOPs of the four panoramas and as well as all the 3D object coordinates of the target points of the Calibration Testfield were jointly refined by applying a bundle adjustment.

## G. Experimental Test – Fort Jargo, Ghana

The MRD algorithm has been tested on a number of cultural heritage sites. An example is Fort Jago, formally known Fort Sao Jago da Mina (Figures 16 and 17). The Fort is in Elmina along the coast in the Central Region of Ghana and was built in the 1660s by the Dutch to protect the Elmina Castle from attacks.

Three panoramas A, B and C were captured at the central court of the Fort Jago. The goal of the experiment was to recover the position of the three panoramas and to subsequently demonstrate the generation of sparse point cloud data.

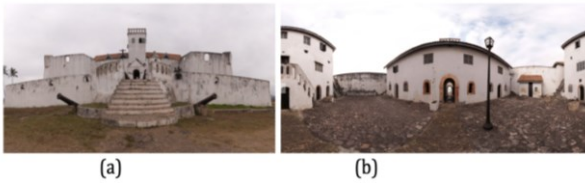


Fig. 16 Images of Fort Jago (a) Front view (b) Central court

International Journal of Engineering Research & Technology (IJERT)
ISSN: 2278-0181
Vol. 13 Issue 06, June - 2024

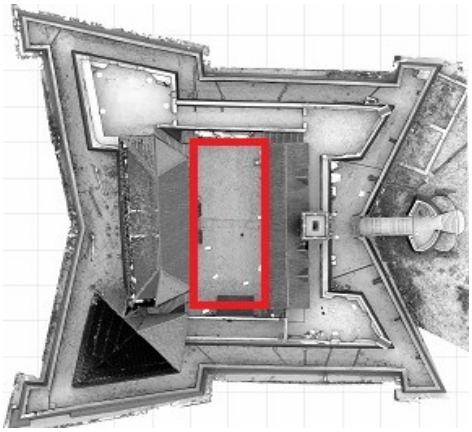

Fig.17 Top view of Fort Jago showing central court area (in red)

Conjugate points required to initiate the orientation process were automatically extracted using the feature-based matching procedure based on the SIFT operator [8, 9]. First, Panorama A was chosen as the reference and sub-divided into five image tiles (Figure 18).

The SIFT operator [8; 9] was applied on Panorama A, B and C to extract feature points. Over 80,000 feature points were extracted from each panorama (Figure 19).


Fig. 18 Panorama A showing the five image tiles

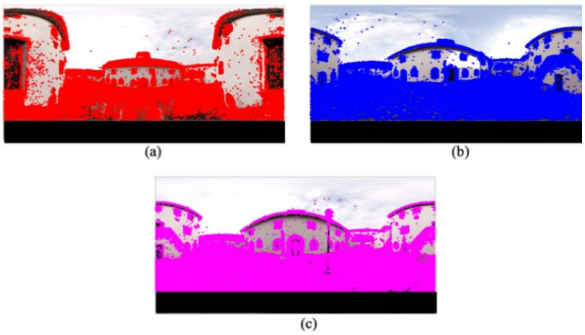


Fig. 19 Extracted feature point using the SIFT operator (a) 82,863 feature points on Panorama A (b) 88,590 feature points on Panorama B (c) 137,675 feature points on Panorama C

Panorama B and C were matched with each of the image tiles in Panorama A after which outliers in the matched features were removed by applying the RANSAC algorithm [10]. Figures 20 shows graphical representation of the matched feature points between Panorama B and the first two image tiles of Panorama A.

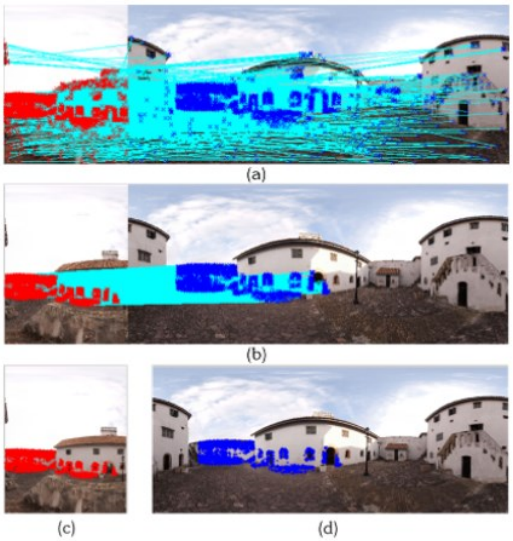


Fig. 20 Results of feature-based matching and outlier detection procedures between Panorama B and the first image tile of Panorama A (a) Feature matching (b) Outlier detection (c) Matched features in first image tile of Panorama A (d) Matched features in Panorama B

A total of 3174 correct matches were obtained from the matching procedure between panorama pair AB. Similar matching procedures was conducted for Panoramas pairs AC and BC. Twenty-five feature points common to the three panoramas were selected as input for the orientation phase. The MRD algorithm was then applied to orient Panoramas B and C to Panorama A after which the derived objects were scaled. The initial approximation values for the position of the three panoramas as well as their orientation parameters and the 3D object coordinates of the twenty-five feature points were then refined with the bundle adjustment algorithm. The panorama positions as well as the 3D object coordinates of all feature points were then refined with the bundle adjustment algorithm.

## III. RESULTS AND DISCUSSIONS

### A. Experimental Results - UCT Calibration Testfield

Table 1 shows the final EOPs of the four panoramas of the Geomatics Laboratory. The EOPs of the panoramas obtained from the MRD algorithm, were compared with their values after bundle adjustment. To provide a good basis for comparison, the bundle adjustment, like the MRD algorithm was also applied to a pair of panoramas at a time. The bundle adjustment algorithm was based on the minimum constraint approach where the seven parameters required to define the datum are held fixed. The parameters that were held fixed in this experiment were the six EOPs of the reference panorama (A) as well as the x-coordinate of the free panorama. This allowed for a direct comparison of the EOPs of the free panoramas. (Tables 2 and 3).

International Journal of Engineering Research & Technology (IJERT)
ISSN: 2278-0181
Vol. 13 Issue 06, June - 2024

TABLE 1 FINAL EOPS OF THE FOUR PANORAMAS OF THE GEOMATICS LABORATORY

| | X (m) | Y (m) | Z (m) | ω (°) | ϕ (°) | κ(°) |
|---|---|---|---|---|---|---|
| A | -0.008 | 0.023 | -0.004 | 0.041 | -0.244 | -0.102 |
| B | 5.361 | -0.418 | 0.306 | -0.492 | 0.577 | 177.367 |
| C | 6.419 | 2.964 | 0.355 | 0.575 | -0.298 | 337.238 |
| D | 1.182 | 2.816 | 0.314 | 0.181 | -0.220 | 353.253 |

The average standard deviations of the seventy-seven 3D object coordinates of calibration target points were estimated as $\sigma_x$=0.7 mm, $\sigma_y$=1.2 mm (depth direction), $\sigma_z$ = 0.6 mm and $\sigma_{xyz}$ = 1.5 mm.

The 3D object positions of the fifteen image points obtained from the MRD and bundle adjustment algorithms were compared with their reference values obtained by survey measurement. The comparison was only possible after applying a 3D Helmert transformation. Four target points served as controls whilst the remaining four were used as check points to verify the accuracy of the object points. Tables 2 and 3 show the comparison bebween the EOPs of the Panorama B and C respectively, after applying MRD and bundle adjustment algorithms. Tables 4 shows the accuracy of the 3D object coordinates of 15 points after applying MRD and bundle adjustment algorithms. From Tables 2 to 4, it can be observed that the 3D positions of Panoramas B and C as well as the 3D object coordinates of the 15 points obtained from the MRD and bundle adjustment algorithms differed in the order of few millimetres.

TABLE 2 COMPARISON OF EOPS FOR PANORAMA B AFTER APPLYING MRD AND BUNDLE ADJUSTMENT ALGORITHMS

| Parameter | MRD | Bundle adjustment | Difference |
|---|---|---|---|
| $X_o$ (m) | 5.383 | 5.383 | 0.00 |
| $Y_o$ (m) | -0.415 | -0.416 | 0.001 |
| $Z_o$ (m) | 0.298 | 0.299 | -0.001 |
| $\omega$ (deg. decimals) | 0.34 | 0.35 | -0.01 |
| $\phi$ (deg. decimals) | -0.37 | -0.36 | -0.01 |
| $\kappa$ (deg. decimals) | -177.72 | -177.74 | 0.02 |

This is an indication that, while the accuracy of the bundle adjustment algorithm was better (Table 4), the MRD algorithm provided good initial approximation values. Should millimetre accuracy be desired, then the initial approximation values obtained from the MRD orientation are sufficient as final values

TABLE 3 COMPARISON OF EOPS FOR PANORAMA C AFTER APPLYING MRD AND BUNDLE ADJUSTMENT ALGORITHMS

| Parameter | MRD | Bundle adjustment | Difference |
|---|---|---|---|
| $X_o$ (m) | 6.436 | 6.436 | 0.000 |
| $Y_o$ (m) | 2.812 | 2.966 | -0.155 |
| $Z_o$ (m) | 0.310 | 0.338 | -0.028 |
| $\omega$ (deg. decimals) | 0.42 | -0.38 | 0.80 |
| $\phi$ (deg. decimals) | -0.11 | 0.18 | -0.29 |
| $\kappa$ (deg. decimals) | 337.52 | 337.47 | 0.05 |

TABLE 4 ACCURACY OF 3D OBJECT POINTS FROM MRD AND BUNDLE ADJUSTMENT ORIENTATION

| Parameter | Orientation of Panorama A, B (mm) | | Orientation of Panorama A, C (mm) | |
|---|---|---|---|---|
| | *MRD* | *Bundle adjustment* | *MRD* | *Bundle adjustment* |
| $\sigma_X$ (mm) | 0.1 | 0.1 | 2.6 | 0.5 |
| $\sigma_Y$ (mm) | 0.5 | 0.5 | 4.2 | 0.2 |
| $\sigma_Z$ (mm) | 0.9 | 0.6 | 9.4 | 2.0 |
| $\sigma_{XYZ}$(mm) | 1.0 | 0.8 | 10.6 | 2.1 |

However, the MRD, unlike the bundle adjustment algorithm can only be applied to a pair of panoramas at a time. It is a well-known fact, the precision of 3D object points as well as the reliability of the photogrammetric network is greatly improved in a multi-image orientation process. Thus, including additional panorama stations will increase network redundancy and the chance of detecting gross and systematic errors. For this reason, as well as the fact that the bundle adjustment algorithm provides improvement to the MRD results, it is advisable to always apply the bundle adjustment after the MRD algorithm.

A further test was carried out on two pairs of panoramas to confirm the effect of weak panorama network configurations on the determination of 3D coordinates of object points. Seventy-seven target points of the Calibration Testfield were used for this test. The test was performed after applying MRD algorithm and the bundle adjustment to panoramas A and B (Figure 21a) as well as to panoramas A and D (Figure 21b). 2 (Panorama A and D) respectively after bundle adjustment.

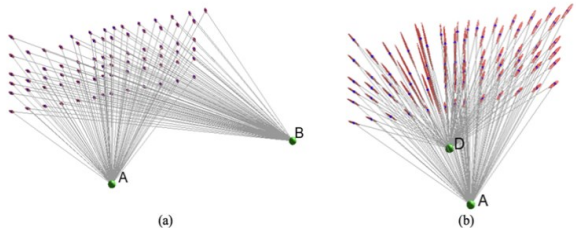


Fig. 21 Comparison between strong and weak network configurations showing error ellipsoids for object points: (a) Network configuration 1 has large B/D ratio, (b) Network configuration 2 has small B/D ratio

Figure 21 and Table 5 show the geometry and the average standard deviation of the seventy-seven object point coordinates from network configuration 1 (Panorama A and B) and network configuration 2 (Panorama A and D).

TABLE 5 COMPARISON OF AVERAGE STANDARD DEVIATIONS OF 77 OBJECT POINT COORDINATES OBTAINED FROM TWO NETWORK CONFIGURATIONS

| Network configuration | $\sigma_X$ (mm) | $\sigma_Y$ (mm) | $\sigma_Z$ (mm) | $\sigma_{XYZ}$ (mm) |
|---|---|---|---|---|
| Network 1 (Panoramas A and B) | 0.1 | 0.3 | 0.1 | 0.4 |
| Network 2 (Panoramas A and D) | 4.4 | 8.1 | 1.2 | 9.3 |

It is well known that large base to-height ratio (B/D) ensures strong geometry in contrast to small B/D. Typical B/D of about 0.5 – 0.75 have been reported to improve precision in the depth direction while B/D ratio of 0.3 or below increases depth error

International Journal of Engineering Research & Technology (IJERT)
ISSN: 2278-0181
Vol. 13 Issue 06, June - 2024

[11-13]. Figures 21a and 21b demonstrates a case of strong geometry with a B/D of about 0.9 and a weak geometry with a B/D of about 0.25 respectively. It can be noted from Table 5 that, as the B/D decreases, the precision of the y-coordinates (depth direction) of the calibration target decreases from 0.3 mm to 8.1 mm. This justifies why the shape of the error ellipsoids in Network configuration 1 is more homogeneous and isotropic than Network configuration 2 (Figure 21).

B. Experimental Results – Fort Jargo, Ghana

The final EOPs of the three panoramas after applying the MRD and bundle adjustment algorithms are provided in Table 6. The average standard deviation of the 3D coordinates of object points after applying bundle adjustment was $\sigma_x$= 0.027 m, $\sigma_y$=0.013 m, $\sigma_z$ = 0.008 m. Figure 22 show the sparse point cloud of central courtyard of Fort Jago derived from the three panoramas.

TABLE 6 FINAL EOPS OF THE THREE PANORAMAS OF THE CENTRAL COURT OF FORT JAGO

| | X (m) | Y (m) | Z (m) | ω (°) | ϕ (°) | κ(°) |
|---|---|---|---|---|---|---|
| A | 0.781 | 0.014 | 0.131 | 0.691 | 0.259 | -1.578 |
| B | 2.642 | -4.627 | -2.424 | 1.898 | 0.244 | 342.768 |
| C | 0.461 | -5.662 | -2.588 | 0.965 | 0.590 | 0.097 |

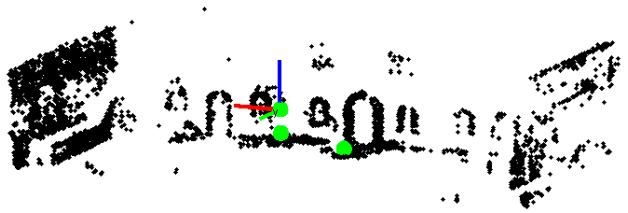

Fig. 22 3D sparse point cloud of central courtyard of Fort Jago

## IV.CONCLUSION

This paper has presented the development and application of the Minimum Ray Distance (MRD) algorithm for accurate orientation of spherical panoramic images. The MRD algorithm is based on the minimisation of distances between two conjugate space vectors or skewed rays by rotating one panorama with respect to a reference panorama. While no information about the relative position and height of the panoramas are known, the MRD algorithm assumes that the panoramas to be oriented are within 10° horizontal or "quasi-horizontal". The integration of MRD with bundle adjustment techniques has demonstrated its effectiveness in generating precise 3D coordinates from spherical panoramas, as validated through experimental tests using a Calibration Testfield and at Fort Jago in Ghana. The extraction of 3D information from spherical panorama proposed in this paper is most appropriate for applications which do not require dense point clouds and in situations with limited access to funds or as a quick field method to document many features in a short time. This is because a single image orientation is required for several overlapping images as compared to the normal stereo or multi-image photogrammetric approach. It is not suggested that 3D reconstruction from spherical panoramic images should replace traditional close-range photogrammetry or laser scanning; rather, that the user of panoramic images will be offered supplementary information to the conventional and modern cultural heritage documentation approaches

## REFERENCES

[1] Luhmann, T. & Tecklenburg, W. 2004. 3-D object reconstruction from multiple-station panorama imagery. Proceedings of ISPRS Workshop on Panorama Photogrammetry. 34(5). Available: http://www.isprs.org/proceedings/5-W16/papers/PanoWS_Dresden2004_Luhmann_b.pdf [2016, January 15].

[2] Maas, H.G. and Schneider, D., 2004. Photogrammetric processing of digital 360 panoramic camera image data. Essee [viitattu 20.8. 2018]. Saatavissa: https://pdfs. semanticscholar. org/b777/7ea82fdfb6b2e654ff0aee7a7b4b5d658246. pdf.

[3] Fangi, G. 2007. The Multi-image spherical Panoramas as a tool for Architectural Survey. XXI International CIPA Symposium. (October):256--1840. Available: http://citeseerx.ist.psu.edu/viewdoc/summary?doi=10.1.1.222.4044 [2016, January 15].

[4] Fangi, G. 2010. Multiscale Multiresolution Spherical Photogrammetry With Long Focal Lenses for Architectural Surveys. International Archives of Photogrammetry, Remote Sensing and Spatial Information Sciences. XXXVIII. Available: http://citeseerx.ist.psu.edu/viewdoc/summary?doi=10.1.1.222.4450&rank=1\nhttp://citeseerx.ist.psu.edu/viewdoc/summary?doi=10.1.1.222.4450&rank=9 [2016, January 15].

[5] Russell, S.J., Norvig, P., Canny, J.F., Malik, J.M. & Edwards, D.D. 2003. Artificial intelligence: a modern approach. V. 2. Prentice hall Upper Saddle River.

[6] Snyder, J.P. 1987. Map Projections: A Working Manual. V. 1395. US Government Printing Office. DOI: 10.2307/1774978.

[7] Fangi, G. & Nardinocchi, C. 2013. Photogrammetric Processing of Spherical Panoramas. The Photogrammetric Record. 28(143):293–311. DOI: 10.1111/phor.12031.

[8] Lowe, D.G. 1999. Object recognition from local scale-invariant features. In Proceedings of the Seventh IEEE International Conference on Computer Vision. V. 2. 1150–1157. DOI: 10.1109/ICCV.1999.790410.

[9] Lowe, D.G. 2004. Distinctive Image Features from Scale-Invariant Keypoints. International Journal of Computer Vision. 60(2):91–110. DOI: 10.1023/B:VISI.0000029664.99615.94.

[10] Fischler, M.A. & Bolles, R.C. 1981. Random sample consensus: a paradigm for model fitting with applications to image analysis and automated cartography. Communications of the ACM. 24(6):381–395.

[11] Fraser, C.S. 1984. Network Design Considerations for Non-Topographic Photogrammetry. Photogrammetric Engineering & Remote Sensing. 50(8):1115–1126.

[12] Remondino, F., Menna, F., Koutsoudis, A., Chamzas, C. & El-Hakim, S. 2013. Design and implement a reality-based 3D digitisation and modelling project. In Proceedings of the DigitalHeritage 2013 - Federating the 19th Int'l VSMM, 10th Eurographics GCH, and 2nd UNESCO Memory of the World Conferences, Plus Special Sessions fromCAA, Arqueologica 2.0 et al. V. 1. 137–144. DOI: 10.1109/DigitalHeritage.2013.6743723.

[13] Voltolini, F., Remondino, F., Pontin, M. & Gonzo, L. 2006. Experiences and Considerations in Image-Based Modeling of Complex Architectures. XXXIV/International Archives of Photogrammetry, Remote Sensing, and Spatial Information Sciences. XXXVI(5):309–314.

[14] Tagoe, N.D., 2017. Developing an accurate close-range photogrammetric technique for extracting 3D information from spherical panoramic images. PhD Thesis, UCT, 1-122